Noname manuscript No.
(will be inserted by the editor)

Implicit finite volume method with a posteriori limiting for transport networks

Matthias Eimer · Raul Borsche · Norbert Siedow

Received: date / Accepted: date

Abstract Simulating the flow of water in district heating networks requires numerical methods which are independent of the CFL condition. We develop a high order scheme for networks of advection equations allowing large time steps. With the MOOD technique unphysical oscillations of non smooth solutions are avoided. In numerical tests the applicability to real networks is shown.

Keywords high order · finite volume method · transport network · district heating · a posteriori limiting · implicit scheme

1 Introduction

The current trend towards renewable energy sources UBA (2020) raises the importance of their efficient use. A fast and accurate simulation of their transport through the distribution network is key to the emerging optimization tasks. The most prominent examples are gas networks, the power grid and district heating networks. In district heating networks hot water is conducted from heat sources, e.g. power plants, to the consumers. As water is incompressible, the governing equation can be split into a hydraulic part, determining the flow of water, and a transport part, which models the advection of the temperature Borsche et al. (2019); Mohring et al. (submitted 2020). The hydraulic system can be solved with methods for differential algebraic systems Cabrera et al. (1995),Wagner (2018). In this article we focus on constructing a suitable numerical method for the transport of the thermal energy.

Matthias Eimer · Norbert Siedow
Fraunhofer ITWM , Fraunhofer Platz 1, 67663 Kaiserslautern, Germany
E-mail: matthias.eimer@itwm.fraunhofer.de

Raul Borsche
Technische Universität Kaiserslautern, Erwin-Schrödinger-Strasse, 67663 Kaiserslautern, Germany

For hyperbolic PDEs a large variety of numerical methods exists LeVeque (1992); Toro (2009). Most of these methods are explicit, which leads to tight restrictions on the time step. In the context of district heating networks such methods have been considered in e.g. Köcher (2000); Grosswindhager et al. (2011). Schemes capable to handle problems with low Mach numbers Boscarino et al. (2018); Zeifang et al. (2019), can relax the restriction due to the hydraulic wave speeds, but not those due to the velocity of the flow ($\approx 1\frac{m}{s}$). As the lengths of the pipes in a network can vary by two orders of magnitude, short tubes can further reduce the time steps size. Local time steps on each pipe can relax this restriction Borsche et al. (2019), but bounds due to the CFL condition remain to tight for practical applications. Avoiding the time step restriction by using Lagrangian approaches, e.g. Iske and Käser (2004); Qiu and Shu (2011), is difficult on networks, since tracing back across the nodes is often challenging or sometimes even impossible.

Only implicit methods are completely without restrictions on the size of the time steps. Here again central schemes can have troubles in finding suitable values at the nodes. Upwind orientated schemes further have the advantage, that their systems can be solved iteratively. First order methods, like the implicit first order upwind scheme, suffer from strong numerical diffusion. A possible high order method is the implicit WENO scheme Arbogast et al. (2019). It achieves good results for moderate CFL numbers around $CFL = 3$ on a single segment. Applied to bigger networks however, the arising nonlinear equations become extremely hard to solve.

In this paper we propose a high order scheme based on a classical finite volume approach. The high order terms reduce significantly the numerical diffusion even for large time steps of $CFL = 10$ and above. The use of a pure upwind stencil enables a straight forward implementation of coupling conditions at the nodes and leads to an iterative solver similar to explicit schemes. It also offers the possibility to use an a posteriori limiting approach, as the values are computed in a successive order. To avoid unphysical oscillations we use a limiting following the idea of the MOOD framework Clain et al. (2018),Clain et al. (2011).
The paper is structured as follows: First, we introduce the mathematical model and the necessary notations. In the third chapter, schemes of 3rd and 4th order are presented and their stability is analyzed. Afterwards we define the a posteriori limiting procedure and introduce a mixed order flux by a convex combination of different orders. The numerical behavior of the scheme is analyzed with Shu's linear test and on a minimal network. Finally, we apply the scheme to a realistic district heating network and show its advantages compared to current state of the art schemes.

2 Model and notations

sec:Model

A district heating network can be described by a directed graph $\mathcal{G} = (\mathcal{V}, \mathcal{E})$ with node set $\mathcal{V}$ and edge set $\mathcal{E} \subset \mathcal{V} \times \mathcal{V}$ of ordered pairs. Following the model in Borsche et al. (2019) to each edge e a spatially constant velocity v_e is assigned. As for our numerical scheme the velocities are constant in time during a time step, we assume all velocities to be positive.This can be achieved by local transformations of edge orientations. Furthermore we define sources $S \subset \mathcal{V}$ as a set of nodes, where

Dirichlet boundary conditions can be imposed. In order to avoid some pathological configurations we further assume:

Assumption 1: The graph $\mathcal{G} = (\mathcal{V}, \mathcal{E})$ is directed acyclic, i.e. there are no directed circles in $\mathcal{G}$
Assumption 2: The graph $\mathcal{G}$ is strongly connected regarding S,
i.e. $\forall V \in \mathcal{V} : V \in S$ or $\exists s \in S$ with V is reachable from s

For every node V, we can identify the set of ingoing edges $\mathcal{I}_V$ and the set of outgoing edges $\mathcal{O}_V$ as

$$\mathcal{I}_V = \{e = (V_1, V_2) \in \mathcal{E} | V = V_1\}, \quad \mathcal{O}_V = \{e = (V_1, V_2) \in \mathcal{E} | V = V_2\}.$$

Each edge e has a corresponding length L_e and is parametrized by $x \in [0, L_e]$. As in the model in Borsche et al. (2019), on every edge e the transport of the quantity u is described by an advection equation with a constant velocity v_e

$$\partial_t u_e + v_e \partial_x u_e = 0 \qquad \forall e \in \mathcal{E} \tag{1}$$

eq:pde

along with suitable initial conditions. In all the nodes $V \in \mathcal{V}$, we assume a linear mixing law of the form

$$\begin{aligned} \sum_{i \in \mathcal{I}_V} v_i u_i(x = L, t) &= \sum_{j \in \mathcal{O}_V} v_j u_j(x = 0, t) \ , \\ u_{j_1}(0, t) &= u_{j_2}(0, t) \qquad \forall\ j_1, j_2 \in \mathcal{O}_V \ . \end{aligned} \tag{2}$$

eq:coupling

The first condition of (2) is the conservation of mass in the hydraulic system, while second one models a homogeneous mixing of u. At the sources Dirichlet boundary conditions at $x = 0$ are imposed.

There are no waves entering the system at the outflow boundaries, thus we do not prescribe any data there. In the application to district heating networks (see section 5) the outflow nodes will be connected to consumers and their measured output acts as input data for the hydraulic solver.

3 Numerical Method

umericlMethods

For problems of type (1) many numerical methods are available Toro (2009), LeVeque (1992). For the application of district heating networks, fast schemes with time steps corresponding to CFL numbers about 20 are required, as large time horizons on networks with largely varying pipe length are considered. Furthermore we seek for high order methods to obtain accurate results even with these large time steps. In the following we focus on finite volume methods of order three and four and incorporate an a posteriori limiter in order to eliminate the unphysical oscillations.

When constructing schemes for conservation laws on networks, central stencils pose some difficulties. In general the coupling conditions are not injective and therefore data in the downwind direction can not be reconstructed at the nodes. Thus we focus on purely upwind based schemes. Since the reconstruction across the nodes is difficult even in the upwind direction we aim for stencils as small as possible.

On every edge of length L we assume a uniform spacial discretization $(x_i)_{i=1,\dots,N}$ with grid size Δx. The global time step is denoted by Δt and the local CFL number is $c = v\frac{\Delta t}{\Delta x}$. For the sake of simplicity, we will drop the edge index in the formulation of the scheme and lower indices will refer to the spacial discretization. Thus the classical update formula of finite volume schemes for the cell averages u_i^{n+1} at time t^{n+1} reads

$$u_i^{n+1} = u_i^n - \frac{\Delta t}{\Delta x}\left(F_{i+\frac{1}{2}} - F_{i-\frac{1}{2}}\right) \qquad i = 1, \dots, N \ ,$$

where $F_{i+\frac{1}{2}}$ are the numerical fluxes at the interfaces.

3.1 Scheme of order 4

sec:4th_order

For a scheme of order P we need to process for the numerical flux at least $d^F = P$ values of u and $d = P + 2$ values for the final update. Thus for a scheme of order 4 the most compact upwind directed stencil for the flux is given by $(u_i^n, u_i^{n+1}, u_{i-1}^n, u_{i-1}^{n+1})$.

As indicated in Figure 1, when solving (1) these values are transported to the vertical time axis at $x_{i+\frac{1}{2}}$ along the characteristics.

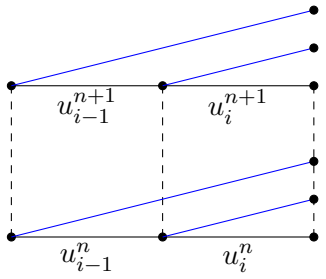

FIG:4th

Fig. 1: Following characteristics to $x_{i+\frac{1}{2}}$

At the interface we perform a conservative interpolation to obtain a polynomial p of order 3 with the constraints

$$\int_{t^n}^{t^n+\frac{\Delta t}{c}} p(\tau)\mathrm{d}\tau = \frac{1}{c}u_i^n \ , \qquad \int_{t^n+\frac{\Delta t}{c}}^{t^n+2\frac{\Delta t}{c}} p(\tau)\mathrm{d}\tau = \frac{1}{c}u_{i-1}^n$$

$$\int_{t^{n+1}}^{t^{n+1}+\frac{\Delta t}{c}} p(\tau)\mathrm{d}\tau = \frac{1}{c}u_i^{n+1} \ , \qquad \int_{t^{n+1}+\frac{\Delta t}{c}}^{t^{n+1}+2\frac{\Delta t}{c}} p(\tau)\mathrm{d}\tau = \frac{1}{c}u_{i-1}^{n+1} \ .$$

The corresponding numerical flux is computed by $F_{i+\frac{1}{2}} = \int_{t^n}^{t^{n+1}} vp(\tau)d\tau$ and has the form

$$F_{i+\frac{1}{2}} = v\left[\left(\frac{c}{12}+\frac{1}{4}+\frac{1}{6c}\right)u_{i-1}^{n} + \left(-\frac{c}{12}+\frac{1}{4}-\frac{1}{6c}\right)u_{i-1}^{n+1} + \left(-\frac{c}{12}+\frac{1}{4}+\frac{5}{6c}\right)u_{i}^{n} + \left(\frac{c}{12}+\frac{1}{4}-\frac{5}{6c}\right)u_{i}^{n+1}\right] .$$

Thus the final scheme reads

$$\begin{aligned} u_i^{n+1} = u_i^n &+ \left(\frac{c^2}{12}+\frac{c}{4}+\frac{1}{6}\right)u_{i-2}^{n} + \left(-\frac{c^2}{12}+\frac{c}{4}-\frac{1}{6}\right)u_{i-2}^{n+1} \\ &+ \left(-\frac{c^2}{6}+\frac{2}{3}\right)u_{i-1}^{n} + \left(\frac{c^2}{6}-\frac{2}{3}\right)u_{i-1}^{n+1} \\ &+ \left(\frac{c^2}{12}-\frac{c}{4}-\frac{5}{6}\right)u_{i}^{n} + \left(-\frac{c^2}{12}-\frac{c}{4}+\frac{5}{6}\right)u_{i}^{n+1} . \end{aligned} \tag{3}$$

eq:schemeOrder4

This method can be obtained via various interpretations, e.g. a slightly different formulation of the same scheme can be found in Steinle (1993), named CTCS. It is written in finite difference form with a central stencil, but with the shift $(u_{i-2}^n, u_{i-1}^n, u_i^n) \to (u_{i-1}^n, u_i^n, u_{i+1}^n)$ the scheme (3) can be transformed to the CTCS.

3.2 Scheme of order 3

Similarly we construct a scheme of order 3. As stencil we just use $(u_i^n, u_i^{n+1}, u_{i-1}^{n+1})$. The numerical flux resulting from the second order polynomial interpolation is

$$F_{i+\frac{1}{2}}^{3} = v\left(\frac{c^2+3c-4}{6c}u_i^{n+1} - \frac{c^2-c}{6c}u_{i-1}^{n+1} + \frac{c+2}{3c}u_i^n\right)$$

and the resulting scheme of order 3

$$\begin{aligned} u_i^{n+1} = u_i^n &- \left(\frac{c^2+3c-4}{6}u_i^{n+1} - \frac{c^2-c}{6}u_{i-1}^{n+1} + \frac{c+2}{3}u_i^n\right) \\ &+ \left(\frac{c^2+3c-4}{6}u_{i-1}^{n+1} - \frac{c^2-c}{6}u_{i-2}^{n+1} + \frac{c+2}{3}u_{i-1}^n\right) \end{aligned}$$

Here we emphasize that the choice of the stencil is not arbitrary. In the following sections we will discuss some aspects of the stability of the above schemes and possible alternative choices, e.g. Table 1.

3.3 Stability

sec:stability

A central basic property of a numerical method is its stability. In the following we discuss the linear stability of the above schemes. They both can be written in the general form

$$Au^{n+1} = Bu^n .$$

First we investigate, as commonly done, the case of periodic boundary conditions. The stability conditions for this case are easily verified, as the resulting matrices are normal. For the case with Dirichlet data, those conditions are no longer sufficient but only necessary for stability, see e.g. Sousa (2009),Kreiss (1962).

For the 4th order scheme the matrix $A \in \mathbb{R}^{N\times N}$ is given by

$$A = \begin{pmatrix} a_0 & & & a_{-2} & a_{-1} \\ a_{-1} & a_0 & & & a_{-2} \\ a_{-2} & a_{-1} & a_0 & & \\ & \ddots & \ddots & \ddots & \\ & & a_{-2} & a_{-1} & a_0 \end{pmatrix}, \tag{4}$$ eq:matrixA

with $a_0 = \frac{1}{6} + \frac{c}{4} + \frac{c^2}{12}$, $a_{-1} = \frac{2}{3} - \frac{c^2}{6}$, $a_{-2} = \frac{1}{6} - \frac{c}{4} + \frac{c^2}{12}$. B has the same form with the coefficients $b_0 = \frac{1}{6} - \frac{c}{4} + \frac{c^2}{12}$, $b_{-1} = \frac{2}{3} - \frac{c^2}{6}$, $b_{-2} = \frac{1}{6} + \frac{c}{4} + \frac{c^2}{12}$. The stability of such systems with circulant matrices comes down to the stability condition

$$\frac{|\lambda_{B,k}|}{|\lambda_{A,k}|} \leq 1 \qquad \forall k = 0, \ldots, N-1 \tag{5}$$ stability

where the eigenvalues have the form

$$\lambda_{A,k} = \sum_{j=0}^{N-1} a_j \omega^{kj} \ , \qquad \lambda_{B,k} = \sum_{j=0}^{N-1} b_j \omega^{kj}$$

for the frequencies $\omega = e^{\frac{2\pi i}{N}}$, see Davis (1979). For our six point stencil we obtain for A

$$\begin{aligned} |\lambda_{A,k}|^2 =& a_0^2 + a_{-1}^2 + a_{-2}^2 + 2\cos(\frac{2\pi k}{N})(a_0 a_{-1} + a_{-1} a_{-2}) \\ &+ \left(4\cos^2(\frac{2\pi k}{N}) - 2\right) a_0 a_{-2} \ . \end{aligned}$$

Since $a_0 = b_{-2}$, $a_{-1} = b_{-1}$ and $a_{-2} = b_0$ it follows directly, that

$$\frac{|\lambda_{B,k}|^2}{|\lambda_{A,k}|^2} = 1 \qquad \forall k = 0, \ldots, N-1 \ .$$

Thus all eigenvalues of the solution operator $A^{-1}B$ have modulus one and therefore the 4th order scheme is unconditionally stable.

For the scheme of order 3, evaluation of the stability condition is more involved, as the symmetry in A and B is missing. Therefore we evaluate (5) numerically to indicate the stability region of the scheme. In Figure 2, the modulus of the eigenvalues is shown for different CFL numbers and $N = 50$. We observe, that for $c < 1$ the modulus is larger than 1 and thus the scheme is instable. For $c > 1$ all eigenvalues are smaller or equal than 1, which indicates stability.

For the following we emphasize that the stability of a scheme can depend on the boundary conditions imposed. Therefore we now discuss the stability of the two schemes in case of Dirichlet boundary conditions. The layout of the matrices

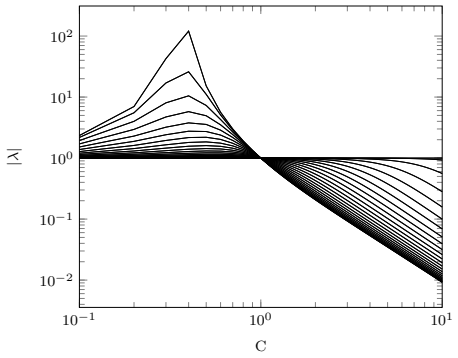

:stability3pbc

Fig. 2: Eigenvalues of $A^{-1}B$ for 3rd order scheme

slightly changes, i.e. compared to (4) the upper right block is eliminated and the matrix $\tilde{A}$ has the form

$$\tilde{A} = \begin{pmatrix} a_0 & & & & \\ a_{-1} & a_0 & & & \\ a_{-2} & a_{-1} & a_0 & & \\ & \ddots & \ddots & \ddots & \\ & & a_{-2} & a_{-1} & a_0 \end{pmatrix} .$$

The new form of $\tilde{B}$ is analogue. These matrices are no longer normal, which implies that the error amplification factor is now measured by the largest singular value of $\tilde{A}^{-1}\tilde{B}$, which is not related to its eigenvalues.

As we did not find any analytical expressions, we rely on a numerical evaluation of the stability regions. In Figure 3 the largest singular value is shown for different matrix sizes N and different CFL numbers.

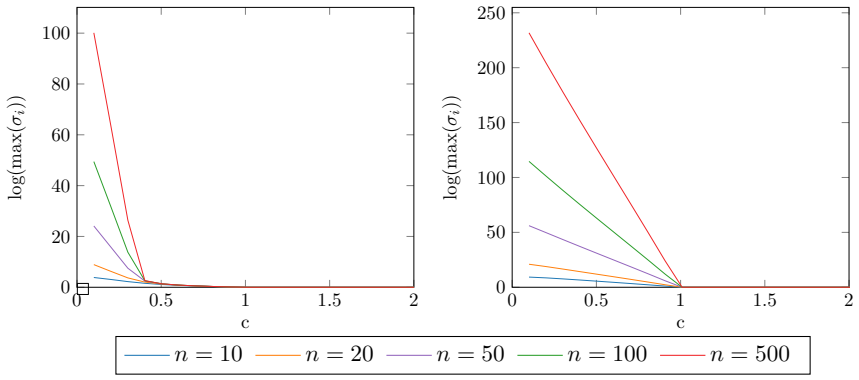

IG:stability_D

Fig. 3: largest singular values of $\tilde{A}^{-1}\tilde{B}$ for the 3rd (left) and 4th (right) order scheme for different n and c.

We observe that both schemes are unstable for $c < 1$, but stable for $c > 1$. Note that for the scheme of order 4 this differs from the case of periodic boundary conditions. Since for $c < 1$ the size of the largest singular value increases with N we do expect this instability to hold for any choice of discretization. Thus both schemes are unstable for $c < 1$. But this is a mild drawback, as in this case a classical explicit method can be used.

Further we applied this analysis on all possible upwind biased combinations of stencils up to order 4. The results are summarized in Table 1.

u_i^{n+1}	u_i^n	u_{i-1}^{n+1}	u_{i-1}^n	order	stable expl.	stable impl.
x	x	x	x	4	✓	✓ ✓
x	x	x		3		✓ ✓
x	x			2	✓ ✓	✓ ✓
x		x		2	✓ ✓	✓ ✓
x			x	2	✓ ✓	
	x	x		2	✓ ✓	
	x		x	2	✓ ✓	
x				1	✓ ✓	✓ ✓
	x			1	✓ ✓	
		x		1		✓

Table 1: Stability of different stencils for periodic (✓) and Dirichlet boundary conditions (✓). Unstable combinations are not listed.

tab:stability

Up to order 2 it is possible to find schemes which are globally stable. For order 3 there is only one stable choice available. In most cases the choice of boundary conditions is not affecting the stability, but for the scheme of order 4 and for a, not very intuitive, first order scheme.

3.4 Coupling

In order to apply the above methods in a network, suitable numerical coupling procedures are needed at the nodes. Following the derivation using polynomials in time at the interfaces, we can directly extend the schemes using the coupling conditions (2). At a node V we denote by p_e the temporal polynomials of all ingoing edges $e \in \mathcal{I}_V$. Thus the temporal evolution of the output is given by

$$p_V(t) = \frac{1}{\sum_{e \in \mathcal{O}_V} v_e} \sum_{e \in \mathcal{I}_V} v_e p_e(t) \ .$$

The flux over the first cell of the outgoing edges is then

$$F_{e,0} = \int_{t^n}^{t^{n+1}} v_e p_V(\tau) \mathrm{d}\tau \ .$$

With this flux the first cell can be updated. For the construction of the flux at the next interface, we furthermore need to fill the required ghost cells at the left boundary. Since we already have a polynomial representation of the mass in time

for the leftmost cell interface, we can reconstruct the cell values as they were derived in 3.1. We set

$$u_{-1}^{n} = c \int_{t^n}^{t^n + \frac{\Delta t}{c}} p_V(\tau)\mathrm{d}\tau \ , \qquad u_{-2}^{n} = c \int_{t^n + \frac{\Delta t}{c}}^{t^n + 2\frac{\Delta t}{c}} p_V(\tau)\mathrm{d}\tau$$

$$u_{-1}^{n+1} = c \int_{t^{n+1}}^{t^{n+1} + \frac{\Delta t}{c}} p_V(\tau)\mathrm{d}\tau \ , \qquad u_{-2}^{n+1} = c \int_{t^{n+1} + \frac{\Delta t}{c}}^{t^{n+1} + 2\frac{\Delta t}{c}} p_V(\tau)\mathrm{d}\tau \ .$$

With these ghost cells, all cells along the edge can be updated.

4 A posteriori limiting

High order schemes tend to show spurious oscillations in the presence of discontinuities or sharp gradients. The oscillations can be suppressed by applying an appropriate limiter. There are different possible approaches for the limiting of implicit schemes. In Arbogast et al. (2019) implicit WENO schemes are proposed, where a spacial WENO reconstruction is combined with an implicit Runge-Kutta scheme. They achieve acceptable results for moderate CFL numbers around $C = 3$, but the scheme involves large nonlinear systems that become harder to solve, the larger C gets.

Another possibility is the use of flux corrected transport techniques Steinle and Morrow (1989), Kuzmin et al. (2012). They include the transport with a monotone scheme and a anti-diffusive correction by some high order term. Especially for large time steps, this ansatz suffers from the large diffusion of the first order solution and also involves solving large nonlinear systems.

We therefore want to make use of the recent a posteriori limiting technique, benefiting from the special structure of our problem. Originally designed for multidimensional finite element schemes, the MOOD paradigm Clain et al. (2018),Clain et al. (2011) can be adapted to our requirements while eliminating most disadvantages of the options above.
The key idea of a posteriori limiting is to begin with the computation of a high order solution. Only if that solution appears to be unsuitable, the limiting is activated and a lower order solution is computed. Whether a solution is suitable can be checked with some (possibly problem specific) criteria.
The basic procedure is the following:

1. compute a high order solution for the next time level
2. check, whether this solution can be accepted (i.e. it does not produce spurious oscillations or negative mass, etc.)
3. if high order solution must be discarded, recompute with a lower order
4. iterate (2.-3.) until a monotone fallback solution is reached or the solution passes the check

In the determination, whether a computed value is suitable, Diot et al propose the following criteria Diot et al. (2012):

Physical Admissibility Detection (PAD):
Most importantly, the solution has to fulfill some basic admissibility criteria in order to ensure that the numerical code does not crash and the variables stay in

a meaningful regime.
A classical physical admissibility condition is positivity of the solution. For our application on district heating networks, we incorporate checks for lower and upper bounds of the energy density. The energy must not fall below the return temperature in order to have a well defined consumer model for example. Possible additional conditions are the check for NaN or INF, indicating that something with the solution went wrong.

While the PAD can detect oscillations overshooting the total range, it does not find the ones near steep gradients with moderate values. Those have to be found by numerically analyzing the computed solution. Using a neighborhood of the current cell and evaluating curvature data, we can distinguish local oscillations from the smooth solution as follows.

Extrema Detector (ED):
If

$$\min(u_{i-1}, u_{i+1}) \leq u_i \leq \max(u_{i-1}, u_{i+1})$$

does not hold, cell u_i is a local extremum. This can be either a true extremum of the solution, a local oscillation or some artifact due to round off errors. If we do not find an extremum, the computed value is considered valid. In presence of an extremum in order to identify the right case, we need to look at the local curvatures next to the cell.
We define

$$C_i(u) = u_i^{''}$$

a discrete approximation to the local curvature (eg. by central difference). The local curvature indicators are defined as

$$\chi_{i,m} = min(C_{i-1}, C_i, C_{i+1}), \qquad \chi_{i,M} = max(C_{i-1}, C_i, C_{i+1})$$

Depending on these indicators, we can distinguish the three cases:

Plateau Detector (PD): If the total curvatures are close to zero, we have found a local plateau, where the extremum arised from floating point errors.

$$max(|\chi_{i,m}, \chi_{i,M}|) < \epsilon_{PD},$$

This means we found a valid solution.

Local Oscillation Detector (LOD):
If the signs of the curvature change, i.e.

$$\chi_{i,m}\chi_{i,M} < 0$$

there is a local oscillation in cell u_i. In order to avoid rounding errors, a relaxed version is used

$$\chi_{i,m}\chi_{i,M} < \epsilon_{LOD}$$

Smoothness Detector (SD):
There is a smooth extremum, if the minimal and maximal curvature are close, i.e.

$$1 \geq \frac{min(|\chi_{i,m}, \chi_{i,M}|)}{max(|\chi_{i,m}, \chi_{i,M}|)} \geq 1 - \epsilon_{SD}$$

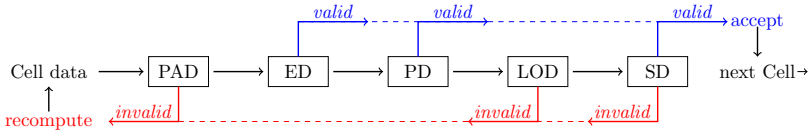

FIG:check

Fig. 4: Admissibility check procedure

The check can be schematically drawn as in Figure 4.

Whenever the check finds 'invalid' cells, the order of the corresponding flux is reduced. Then the check is performed again with the new cell data. We use a cascade of 3 schemes with the orders $4 \to 3 \to 1$, where the high order schemes are as described above and the first order scheme is the implicit upwind scheme, which always produces valid results.

Discrete Maximum Principle (DMP):
An important criterion for most numerical schemes is the satisfaction of a discrete maximum principle. This is a very powerful tool for the detection of spurious oscillations, as the high order overshoots would violate the DMP and can therefore be eliminated. For the application of implicit schemes on transport equations however, we do not have a discrete maximum principle. The long travel distance of cell values makes it impossible to state bounds for the solution. This is why we have to drop the DMP check from our procedure.

4.1 Extrapolation and computation of downwind data for MOOD check

The input data required by the MOOD check consists of at least the cell values $(u_{i-1}^{n+1}, u_i^{n+1}, u_{i+1}^{n+1})$ in order to perform the ED step. That means additionally to the computed candidate solution u_i^{n+1} we have to provide the next cell value as well. While inside the domain, we have access to u_{i+1}^n and the computation of the new cell value at $i+1$ is possible. Note here, that this new data has to be computed with the same order as the value to be checked.
While at the boundary, i.e. at the last cell of any edge in the network however, we do not have the data required to compute another cell value. In this case, we have to extrapolate u_{i+1}^{n+1} only using values inside the domain. Note that also here we require an accuracy of the same order than used before. The numerical flux functions we use are:

$$F_c^4 = v\left(\frac{-c^2+3c+10}{24}u_{i-1}^{n+1} + \frac{c^3+19c+18}{12c}u_i^{n+1} + \frac{-c^3-2c^2+13c+62}{24(c-1)}u_{i+1}^{n+1} + \frac{c^2+5c+6}{4(c-1)c}u_i^n\right)$$

for the 4th order and

$$F_c^3 = v\left(-\frac{c^2+3c+4}{6c}u_i^{n+1} + \frac{c^2-13}{6(c-1)}u_{i+1}^{n+1} + \frac{c^2+3c+2}{3(c-1)c}u_i^n\right)$$

for the 3rd order.

4.2 Convex combination of high order fluxes

The classical MOOD strategy determines the order of the spacial reconstruction polynomial for a given cell. Therefore there is a hard switch of the corresponding fluxes, when the order is decreased. Since we are using the strategy directly on the fluxes, a continuous transition between the different orders is possible. Whenever the order for a given cell has to be reduced from order 4 to order 3 and the 3rd order solution is suitable, we might aswell use a flux of the form

$$F = \alpha F^4 + (1-\alpha)F^3$$

The parameter α can then be chosen in a way, such that

$$\alpha^\star = max\{\alpha | u_i^{n+1} \text{satisfies the MOOD check}\}$$

Unfortunately, this optimization problem is discontinuous, as the MOOD check will only return TRUE or FALSE. The parameter α here is determined by a bisection method. The incorporation of sufficient criteria for the check result into the optimization might accelerate the process.
Altogether, we have constructed a hybrid scheme taking advantage of the monotonicity of the first order upwind aswell as the good approximation quality of the high order ones.

5 Application to district heating networks

sec:appl_dh

We designed this scheme for the application of district heating networks. A district heating network can be modeled by a graph describing the connection between the different components. The edges include the pipes, consumers and the source. In the nodes the coupling conditions between the different components are formulated. In Borsche et al. (2019) and Mohring et al. (submitted 2020) the modeling of such networks is described in more detail. Here we want to restrict ourselves to the solution of the energy advection problem. The system consists of a network of advection equations

$$\partial_t e + v\partial_x e = 0$$

as introduced in (1) and (2). The transported quantity is the energy density e and we will ignore source terms modeling thermal losses for now. As described in Borsche et al. (2019), the velocity for the system is solved separately in every time step by an equation of the form

$$g(v, e, Q) = 0,$$

where Q contains the demand of the consumers of the network. The energies at the outflow nodes of the network are measured (see section 2) and the new velocities are set to fulfill the demand of all consumers given the measured output. This kind of system can efficiently be solved, see Köcher (2000),Jansen and Pade (2013). To

conclude, a splitting technique is used, where in every time step, we get an actualized velocity depending on the old energy densities and current consumption. This results in a first order approximation of the full system. As the largest numerical errors are due to diffusive effects of the energy transport, the overall error is still much lower than a classical first order scheme for the full system.

6 Numerical Examples

ericalExamples

In this section we analyze the constructed schemes in four different test cases. First a classical test case for schemes for hyperbolic conservation laws, Shu's linear test Jiang and Shu (1996), is performed and the convergence is investigated numerically. The third test case is a small example of a network, where during the simulation velocities change their sign. An analytic solution of this case is given in Mohring et al. (submitted 2020). The last test is a part of an existing network geometry with realistic parameters and boundary conditions. We can show that in all cases the new scheme is superior to a classical first order scheme.

6.1 Shu's linear test

The scheme is tested on a 1D domain, with transport velocity $v = 1$ and a demanding initial condition Jiang and Shu (1996). Due to the iterative structure of the scheme, we cannot use it with periodic boundary conditions (see section 3.3). Therefore we extend the spacial domain to from $[0, 1]$ to $[0, 2]$ and initialize the new values with 0. A 0-Dirichlet boundary condition is prescribed at $x = 0$.
In Figure 5, the solution is shown for the time $t = 1$ with hybrid scheme (red) and the unlimited first, third and fourth order schemes (dashed) with $n = 200$ and a CFL number of $c = 2.5$.

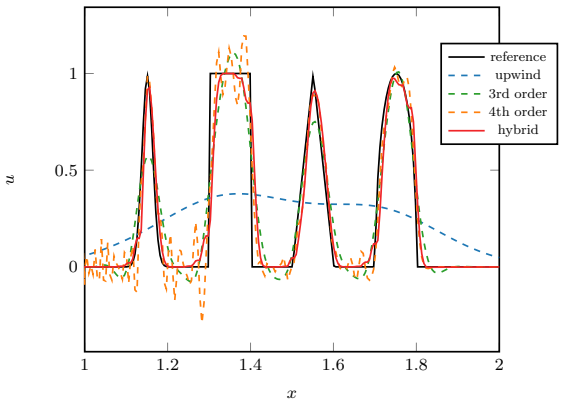

fig:Shu_2

Fig. 5: Shu's linear test with $n = 200, CFL = 2.5$ for different schemes

Compared to the exact solution (black) we can see that the first order solution looses any contour. The unlimited high order schemes, while being more accurate show oscillations near the steep gradients of the exact solution. These oscillations can be removed by the proposed a posteriori limiting strategy of the hybrid scheme.

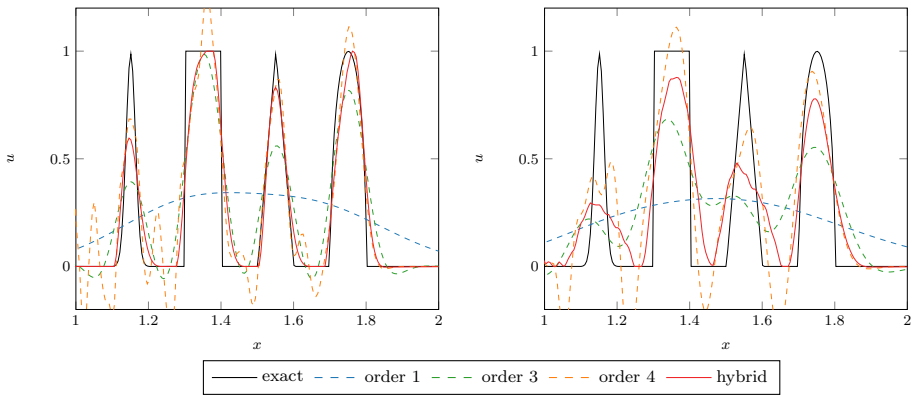

Fig. 6: Shu's linear test with CFL numbers 5 and 10. The proposed scheme (red) approximate the exact solution (black).

fig:Shu_1

In Figure 6, we show the behavior of our scheme for different CFL numbers c. In all cases, we can observe the cancellation of overshoots in the whole domain. As the 4th order scheme is exact for $c = 2$, we can expect accurate results for $c = 2.5$. Even there, we notice that the upwind scheme is smearing out almost all the information from the initial condition. As expected, the numerical diffusion rises with larger time steps, but even for $c = 10$, we can distinguish the four peaks and the resulting heights produced by the hybrid scheme are a good compromise between fourth and third order approximations.

6.2 Convergence analysis

In another test case, we provide smooth initial conditions and check the theoretical order of convergence of the scheme. As for smooth data and small enough discretization the MOOD step should not trigger a recalculation, the scheme fully uses the high order fluxes and therefore achieves 4th order accuracy. We use an initial condition of the form

$$u_0(x) = \begin{cases} \sin^4(4\pi x), & \text{if } x \in [0, 0.5] \\ 0, & \text{else} \end{cases}$$

and transport it with $v = 1$ and $CFL = 5$ until $t_{end} = 0.5$.

The convergence rate of 3 different variations of our proposed scheme is shown in Figure 7. With '*hybrid*3' we denote a variation, where we only use the 3rd and 1st order fluxes as high and low order respectively, without application of the convex combination. Furthermore, with '*hybrid*4' we indicate the use of the full cascade $4 \to 3 \to 1$ but also without convex combination. Finally, '*hybrid*' shows

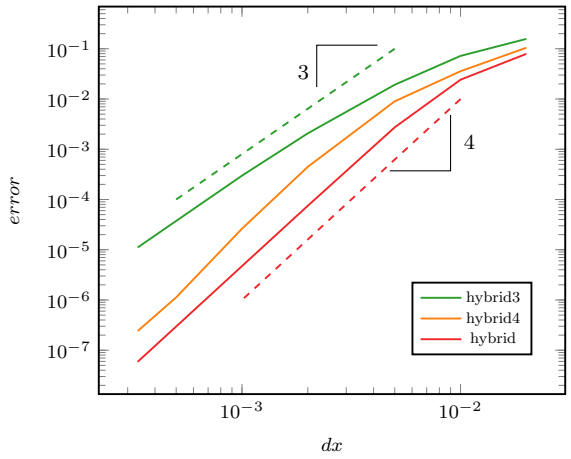

Fig. 7: Error convergence plot

ig:convergence

the results for the full scheme described above. For a course grid, a mild limiting is still active. As the grid is refined we can see that for smooth data all the schemes perform at their theoretical order of convergence.

6.3 Limitations of the scheme

For explicit methods the MOOD approach guarantees certain properties by design. However with the implicit method, there are cases, where the solution with the limiter applied still produces overshoots. This is due to the fact, that the flux orders are chosen sequentially throughout the domain. It is possible, that a choice at some point in the domain may locally fulfill the smoothness test but produces problems a few cells further downstream. The limited window of available data for the check makes it impossible to predict these cases. A possible way out would be an iteration process with backtracking elements to eliminate these cases. In practical applications however, this might imply a huge growth in computation times. For our application on district heating networks, it is not essential to avoid all small overshoots inside the range of admissible temperature values. When the total temperature however gets below a minimal value, the system is not solvable anymore and in these cases, such a mechanism has to be implemented. In realistic settings however this does not happen as near such points, the resulting velocities and pressures would tent to infinity. In real applications, there always is a margin between true solution and the set of solutions that are not admissible.

6.4 Triangle Network

The first network is forming a simple triangle. It contains three pipes and two consumers. For this network, there is an analytical solution available, which produces a flow reversal and therefore a discontinuity in energy while having continuous

boundary- and initial conditions. The details about the solution can be found in Mohring et al. (submitted 2020).

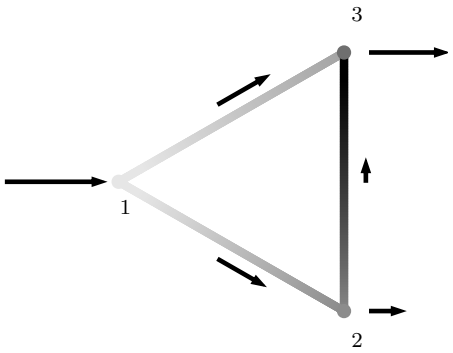

triangle

Fig. 8: Triangle network

The geometry and initial flow directions are shown in Figure 8. The source is located at the left and the two consumers are connected to the two nodes at the right side respectively. A time dependent consumer behavior, where the situation continuously changes from the upper consumer demanding more energy than the lower one to a situation vice versa causes a change in flow direction on the vertical pipe to the right. The initial condition is outlined by the brightness on the edges, brighter meaning higher temperature.

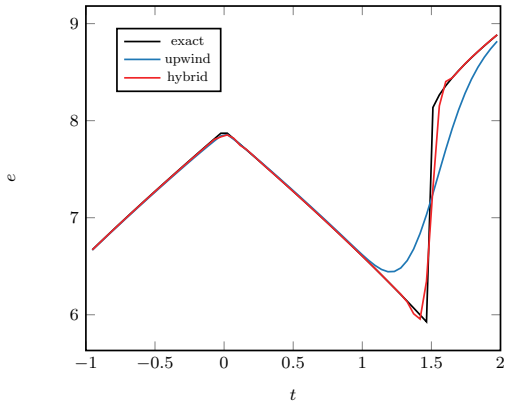

triangle_1

Fig. 9: Temperature signal in node 2

The results of the temperature evolution of the vertical edge at the lower consumption node are shown in Figure 9. The general behavior of the exact solution can be explained as follows: starting from the initial condition, the rising infeed temperature enters the pipe. When the change of flow direction is reached, the temperature decreases again, as the values further down that pipe return to the

node they have passed before. At the same time, at the upper node of that edge, new, hot water enters the pipe, inducing a discontinuity traveling downwards. At some point this discontinuity reaches the lower end of that edge. Thereafter we have a linear behavior again.

In Figure 9 we can see that the hybrid scheme is able to resolve the jump much sharper than the implicit upwind scheme. A significant increase in accuracy of the jump height and the left side value are apparent. For this example, the exact velocity description in time is used for all the schemes. When the advection solver is furthermore coupled to the flow solving algorithm, a precise estimate for the temperatures at the consumers is even more important as it will influence the flow velocities for the next time steps.

6.5 Street network

The street network is a part of a real district heating network. It contains 162 pipes and 32 consumers. The total pipe length is 1672m with the largest pipe measuring 80m and the shortest having 0.06m. Even though not being obvious from the topology plot Figure 10, it does contain one cycle near the label C_2. In the figure, we can see a temperature front traveling through the network. For the pipes, red color means hotter water, blue is cooler water. The dots represent the consumers with the color coding the mass flow from high (red) to low (blue). The solution shown here was solved by an implicit upwind scheme, to demonstrate the smearing of the sharp front inside the network. The initial condition in the network was $T_0 = 80°C$ and the boundary condition at the source is set to

$$T_B = \begin{cases} 100°C, \text{if } t < 1000 \\ 80°C, \text{else.} \end{cases}$$

We want to focus especially on the two consumers marked by red circles, C_1 and C_2.

In Figure 11, we see the temperature signal in time at the rightmost node (C_1) of the network. The resolution for all schemes is $\Delta x = 0.5$m and $\Delta t = 5$s. Since we do not have an analytic description of the solution, the reference is computed by the upwind scheme with 50 times finer resolution ($\Delta x = 0.01$m and $\Delta t = 0.1$s). We can see, that the plain fourth order scheme does not produce stable results due to the extremely high oscillations in front of the shock. The upwind scheme heavily smears out the discontinuity. The hybrid scheme however accurately resolves position and height of the traveling front.

The advantage of the hybrid scheme becomes even more evident when looking at the solution at the consumer furthest away from the source (C_2). The more accurate we can compute the temperatures at the consumers, the better the resulting velocities for the next time steps. Large errors in the temperature may therefore lead to completely different flow fields and consequently different looking solutions. This is even more important when there are circles in the network, that can possibly change their flow direction. Such a case can be seen in Figure 12. Several flow changes and different mixing ratios lead to a rather complicated temperature signal entering the consumer C_2. We can see that compared to the reference solution, the upwind scheme loses most of the dynamics. The solution of the plain fourth order scheme is omitted, since it too oscillatory to give any

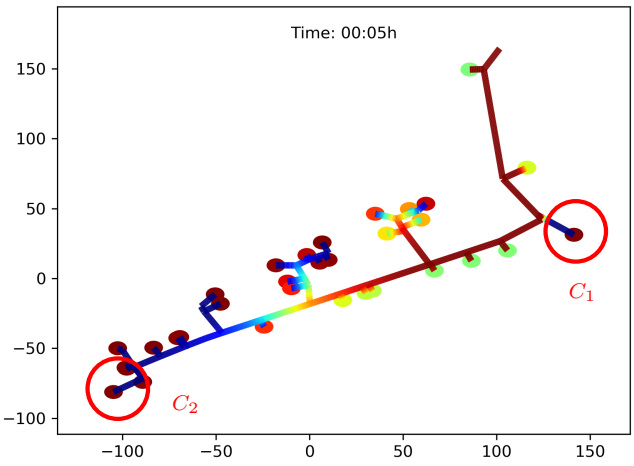

`street`

Fig. 10: Street network topology

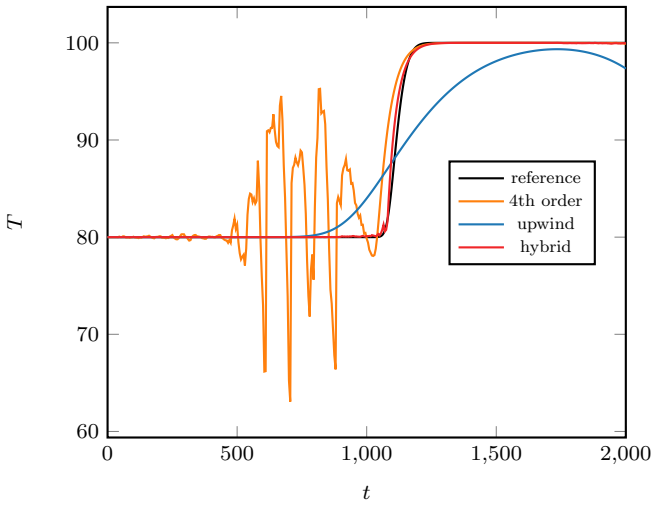

`street_190`

Fig. 11: Temperature signal for consumer C_1

meaningful contribution. The hybrid scheme however accurately resolves all the kinks and waves we observe in the reference solution. For a precise simulation of such networks, it seems evident that high order approaches like this are much more powerful than a straight forward first order approach.

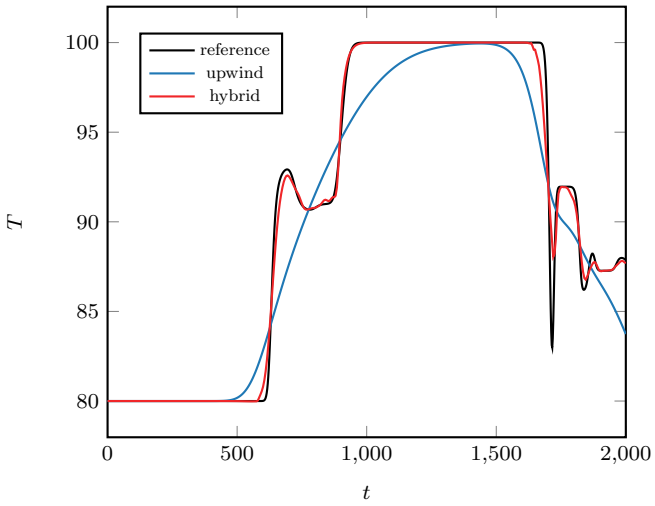

street_189

Fig. 12: Temperature signal for consumer C_2

7 Conclusion

We constructed a high order implicit scheme for district heating networks. The used stencil is upwind orientated, as at the coupling points the data cannot be reconstructed properly, due to the non-injective mixing at the nodes. Furthermore, the upwind orientation allows that the solution can be computed successively without solving large systems of equations. The oscillatory behavior of the high order is massively reduced by an a posteriori limiting approach. Even though overshoots cannot always be avoided by this ansatz, the results show a big improvement of the achieved solutions. Compared to a first order approach the constructed scheme achieves a higher precision on coarser grids and larger time steps.

Acknowledgements The authors acknowledge the financial support by the Federal Ministry of Education and Research of Germany in the framework of the project *EiFer: Energieeffizienz durch intelligente Fernwärmenetze* (grant number 05M18AMB).

Conflict of interest

The authors declare that they have no conflict of interest.

References

iWENO1 Arbogast T, Huang CS, Zhao X (2019) Von neumann stable, implicit, high order, finite volume weno schemes

LTS Borsche R, Eimer M, Siedow N (2019) A local time stepping method for thermal energy transport in district heating networks. Applied Mathematics and Computation 353(C):215–229, DOI 10.1016/j.amc.2019.01.072, URL https://ideas.repec.org/a/eee/apmaco/v353y2019icp215-229.html

Boscarino2018 Boscarino S, Russo G, Scandurra L (2018) All mach number second order semi-implicit scheme for the euler equations of gas dynamics. Journal of Scientific Computing 77(2):850–884, DOI 10.1007/s10915-018-0731-9, URL https://doi.org/10.1007/s10915-018-0731-9

Cabrera1995 Cabrera E, Garcia-Serra J, Iglesias PL (1995) Modelling Water Distribution Networks: From Steady Flow to Water Hammer, Springer Netherlands, Dordrecht, pp 3–32. DOI 10.1007/978-94-017-1841-7_1, URL https://doi.org/10.1007/978-94-017-1841-7_1

MOOD2 Clain S, Diot S, Loubère R (2011) A high-order finite volume method for hyperbolic systems: Multi-dimensional Optimal Order Detection (MOOD). Journal of Computational Physics pp 0–0, DOI 10.1016/j.jcp.2011.02.026, URL https://hal.archives-ouvertes.fr/hal-00518478

MOOD1 Clain S, Loubère R, Machado GJ (2018) a posteriori stabilized sixth-order finite volume scheme for one-dimensional steady-state hyperbolic equations. Advances in Computational Mathematics 44(2):571–607, DOI 10.1007/s10444-017-9556-6, URL https://doi.org/10.1007/s10444-017-9556-6

davis Davis P (1979) Circulant Matrices. New York (N.Y.) : Wiley

MOOD3 Diot S, Clain S, Loubère R (2012) Improved detection criteria for the multi-dimensional optimal order detection (mood) on unstructured meshes with very high-order polynomials. Computers & Fluids 64:43 – 63, DOI https://doi.org/10.1016/j.compfluid.2012.05.004, URL http://www.sciencedirect.com/science/article/pii/S0045793012001909

Grosswindhager Grosswindhager S, Voigt A, Kozek M (2011) Linear finite-difference schemes for energy transport in district heating networks. Proceedings of the 2nd International Con-ference on Computer Modelling and Simulation pp 5 – 7

Iske2004 Iske A, Käser M (2004) Conservative semi-lagrangian advection on adaptive unstructured meshes. Numerical Methods for Partial Differential Equations 20(3):388–411, DOI 10.1002/num.10100, URL https://doi.org/10.1002/num.10100

JP2013 Jansen L, Pade J (2013) Global unique solvability for a quasi-stationary water network model. Preprint series: Institut für Mathematik, Humboldt-Universität zu Berlin 2013-11, URL https://www.mathematik.hu-berlin.de/de/forschung/pub/P-13-11

Jiang1996 Jiang GS, Shu CW (1996) Efficient implementation of weighted ENO schemes. Journal of Computational Physics 126(1):202–228, DOI 10.1006/jcph.1996.0130, URL https://doi.org/10.1006/jcph.1996.0130

koecher2000 Köcher R (2000) Beitrag zur berechnung und auslegung von fernwärmenetzen. PhD thesis, Technische Universität Berlin, http://dx.doi.org/10.14279/depositonce-180

Kreiss1962 Kreiss HO (1962) Über die stabilitätsdefinition für differenzengleichungen die partielle differentialgleichungen approximieren. BIT 2(3):153–181, DOI 10.1007/bf01957330, URL https://doi.org/10.1007/bf01957330

kuzmin Kuzmin D, Löhner R, Turek S (eds) (2012) Flux-Corrected Transport. Springer Netherlands, DOI 10.1007/978-94-007-4038-9, URL https://doi.org/10.1007/978-94-007-4038-9

LeVeque1992 LeVeque RJ (1992) Numerical Methods for Conservation Laws. Birkhäuser Basel, DOI 10.1007/978-3-0348-8629-1, URL https://doi.org/10.1007/978-3-0348-8629-1

KOMSO Mohring J, Linn D, Eimer M, Rein M, Siedow N (submitted 2020) District heating networks - dynamic simulation and optimal operation. In: Mathematical MSO for Power Engineering and Management

Qiu2011 Qiu JM, Shu CW (2011) Conservative high order semi-lagrangian finite difference WENO methods for advection in incompressible flow. Journal of Computational Physics 230(4):863–889, DOI 10.1016/j.jcp.2010.04.037, URL https://doi.org/10.1016/j.jcp.2010.04.037

Sousa2009 Sousa E (2009) On the edge of stability analysis. Applied Numerical Mathematics 59(6):1322–1336, DOI 10.1016/j.apnum.2008.08.001, URL https://doi.org/10.1016/j.apnum.2008.08.001

Steinle1989 Steinle P, Morrow R (1989) An implicit flux-corrected transport algorithm. Journal of Computational Physics 80(1):61–71, DOI 10.1016/0021-9991(89)90090-9, URL https://doi.org/10.1016/0021-9991(89)90090-9

finitediff Steinle PJ (1993) Finite difference methods for the advection equation

Toro2009 Toro EF (2009) Riemann Solvers and Numerical Methods for Fluid Dynamics. Springer Berlin Heidelberg, DOI 10.1007/b79761, URL https://doi.org/10.1007/b79761

energy UBA (2020) german environment agency: Erneuerbare Energien in Deutschland

tuprints7252 Wagner L (2018) Second-order implicit methods for conservation laws with applications in water supply networks. PhD thesis, Technische Universität, Darmstadt, URL http://tuprints.ulb.tu-darmstadt.de/7252/

IMEX2 Zeifang J, Schütz J, Kaiser K, Beck A, Lukáčová-Medvid'ová M, Noelle S (2019) A novel full-euler low mach number imex splitting. Communications in Computational Physics 27(1):292–320, DOI https://doi.org/10.4208/cicp.OA-2018-0270, URL http://global-sci.org/intro/article_detail/cicp/13323.html